# Prototype Sodium-Ion Batteries Using an Air-Stable and Co/Ni-Free O3-Layered Metal Oxide Cathode

*Linqin Mu, Shuyin Xu, Yunming Li, Yong-Sheng Hu,* Hong Li, Liquan Chen, and Xuejie Huang*

Large-scale electrical energy storage systems are one of the core technologies in renewable energies and smart grid, among which sodium-ion batteries show great promise due to the abundant sodium resources. Layered metal oxides (of general formula: $A_xMO_2$, where A = Li, Na; M = Co, Ni, Mn, Cr, Fe, etc.) with alternating alkali metal layer and transition metal layer have long been of particular interest since the early 1980s as an important class of cathode materials for rechargeable batteries due to their easy synthesis and high energy density.[1] One of the most successful examples is $LiCoO_2$,[1a] which is commonly used as a cathode in lithium-ion batteries with the highest volumetric energy density for portable electronic devices. Its metal substituted materials ($LiCo_{1-x-y-z}Ni_xMn_yAl_zO_2$) are being used in power batteries for electric vehicles. In the case of sodium-ion batteries operated at room temperature which are proposed for large-scale electrical energy storage owing to the naturally abundant sodium resources in recent years.[2,3] $Na_xCoO_2$ that can electrochemically and reversibly intercalate Na is the first example,[1b] then a large number of layered metal oxides have been extensively exploited.[4–12] However, the practical applications have been hindered by two major challenges. First, unlike $LiMO_2$, almost all the $Na_xMO_2$ are not stable against moisture (either they can be oxidized by water or water/carbon dioxide molecules can be intercalated into alkali metal layer).[4–9,11,12] This will not only increase the substantial cost for material storage, transportation, and battery production but also lead to the inconsistency of the battery performance. Therefore, it is extremely important to explore air-stable layered oxides in the viewpoint of practical applications. Second, although significant progress has been made in new layered metal oxides with abundant elements such as Fe and Mn to form $Na_xFe_{1-y}Mn_yO_2$, their Na storage performance is not satisfactory.[7] It is necessary to incorporate toxic Ni or Co into transition metal layer to achieve better performance.[4–6,8,9] However, as noted above, Ni or Co is widely used in lithium-ion batteries, particularly, with the growing market of electric vehicles, the cost of Ni or Co will definitely increase. Therefore, this is not a good choice for sodium-ion batteries and it is essential to explore Ni/Co-free layered oxides with superior performance. Aiming to address these two problems, here we report an air-stable and Co/Ni-free layered metal oxide of O3-$Na_{0.9}[Cu_{0.22}Fe_{0.30}Mn_{0.48}]O_2$. This material is able to store a reversible capacity of ≈100 mAh $g^{-1}$ at an average storage voltage of 3.2 V with long cycle life. When coupled with hard carbon anode, a prototype rechargeable sodium-ion battery offers an energy density of 210 Wh $kg^{-1}$, a round-trip energy efficiency of 90%, high rate capability, and excellent cycling stability. These desired performances make this system to be closer to the level of practical applications.

The $Na_{0.9}[Cu_{0.22}Fe_{0.30}Mn_{0.48}]O_2$ ($Na_{0.9}[Cu^{II}_{0.22}Fe^{III}_{0.30}Mn^{III}_{0.16}Mn^{IV}_{0.32}]O_2$) material was synthesized by a simple solid-state reaction at 850 °C in air atmosphere using precursors of $Na_2CO_3$, CuO, $Fe_2O_3$, and $Mn_2O_3$. The crystal structure of the as-synthesized material was determined by X-ray diffraction (XRD) as shown in **Figure 1**a together with its refinement results by the Rietveld method (see Table S1, Supporting Information). It can be seen that all the Bragg diffraction peaks are in excellent agreement with the JC DS No. 01-082-1495 (O3-type $\alpha$-$NaFeO_2$) and can be indexed to a hexagonal layered structure with a space group of $R\bar{3}m$, indicative of a typical O3-type layered structure (note that the letter "O" refers to the Na coordination environment of octahedral site whereas the number "3" refers to the number of $MO_2$ slab according to Delmas' notation.[13] A schematic illustration of the O3-type structure is also shown in Figure 1b. The structure refinement gives the lattice parameters $a$ = 2.9587(7) Å, $c$ = 16.3742(6) Å. The lattice parameter of $c$-axis is slightly larger than that of other O3-type materials[5f–h,6b,8a] because the Na content is less than 1. The inductively coupled plasma (ICP) result confirms the composition of $Na_{0.89}[Cu_{0.22}Fe_{0.30}Mn_{0.48}]O_2$ (see Table S2, Supporting Information). The morphology of the resulting sample is shown in Figure 1c. The distribution of the particle size is in the range of 10–30 μm with about 3 μm sized primary particle agglomerations together (Figure 1d). Most importantly, unlike other O3-type materials,[4–9,12] this material is very stable against water. In order to confirm this, we intentionally design an accelerated aging experiment as described in the Experimental Section which was verified by $LiMO_2$ as shown in Figure S1 (Supporting Information). We placed the as-synthesized material in deionized water for 3 d and then dried the material at 100 °C for overnight. The obtained material was checked by XRD again. It can be seen that the XRD pattern is nearly identical to that of the as-synthesized material, which is very different from other O3-type materials as shown in Figure S2 (Supporting Information). These results suggest that the O3-$Na_{0.9}[Cu_{0.22}Fe_{0.30}Mn_{0.48}]O_2$ is very stable against water. Furthermore, after the material was stored in air for one month

L. Q. Mu, S. Y. Xu, Y. M. Li, Prof. Y.-S. Hu, Prof. H. Li, Prof. L. Q. Chen, Prof. X. J. Huang
Key Laboratory for Renewable Energy
Beijing Key Laboratory for New Energy Materials and Devices
National Laboratory for Condensed Matter Physics
Institute of Physics
Chinese Academy of Sciences
Beijing 100190, China
E-mail: yshu@aphy.iphy.ac.cn

DOI: 10.1002/adma.201502449

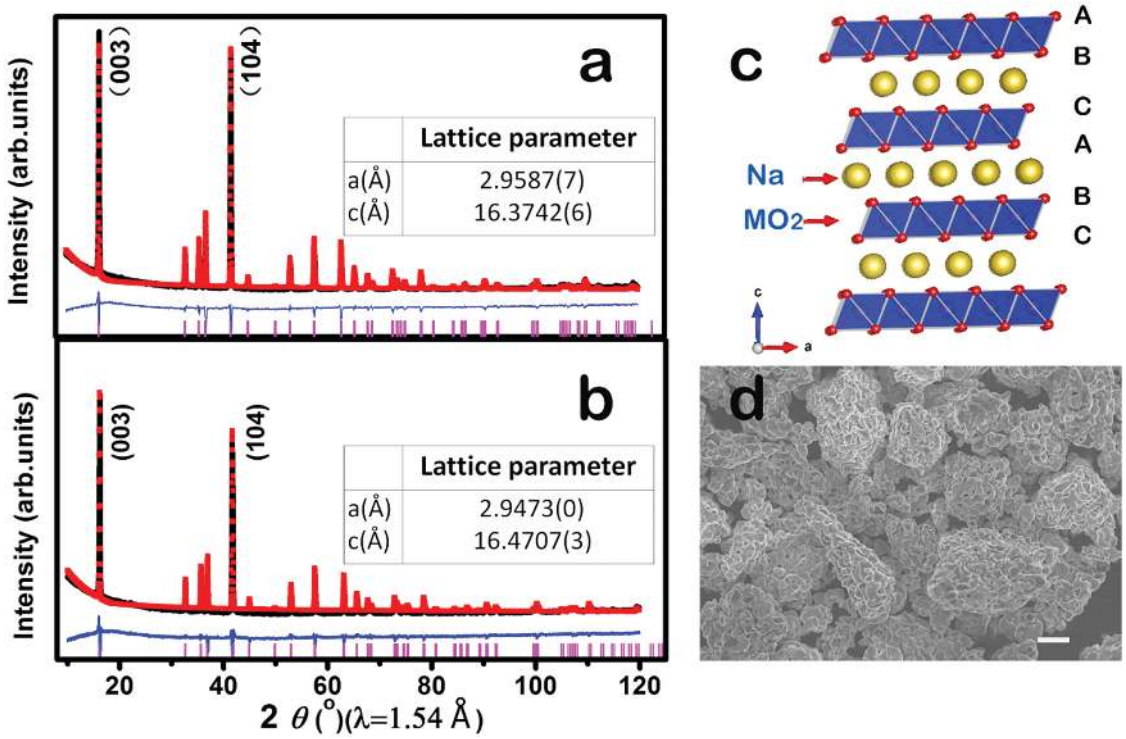


**Figure 1.** Structure of O3-$Na_{0.9}[Cu_{0.22}Fe_{0.30}Mn_{0.48}]O_2$. X-ray diffraction pattern and Rietveld refinement of the a) as-prepared $Na_{0.9}[Cu_{0.22}Fe_{0.30}Mn_{0.48}]O_2$ sample and b) after soaked into water. The black (red) line represents the experimental (calculated) data. The residual discrepancy is shown in blue. The inset tables are the lattice parameters obtained from Rietveld refinement. c) Schematic illustration of the O3-$Na_{0.9}[Cu_{0.22}Fe_{0.30}Mn_{0.48}]O_2$ projected in *a*–*c* plane (left down is projected in *a*–*c* plane). Symbols A, B, and C refer to the different oxygen layers. The blue layer represents the $MO_2$ layer and yellow bullets refer to $Na^+$ ions. d) The typical scanning electron image of as-prepared sample (scale bar is 10 μm).

to exclude the effect of $CO_2$ as a recent work shows that some O3-type oxides are sensitive to $CO_2$ in moisture,[12] neither the crystal structure nor the morphology changes significantly (Figure S3, Supporting Information).

The electrochemical performance of the O3-$Na_{0.9}[Cu_{0.22}Fe_{0.30}Mn_{0.48}]O_2$ electrode was first evaluated in sodium half cells at room temperature. **Figure 2**a shows the galvanostatic charge (Na deintercalation)/discharge (Na intercalation) curves in a voltage range of 2.5–4.05 V versus $Na^+$/Na at a current rate of 0.1C (10 mA $g^{-1}$). A reversible storage capacity of around 100 mAh $g^{-1}$ is achieved with an initial Coulombic efficiency of 90.4%, corresponding to 0.4 $e^-$ transfer. The average storage voltage is 3.2 V. A short voltage plateau at 3.05 V was observed in the charge and discharge process, suggesting a phase transition occurring in this O3-type material as discussed later. When comparing the first two charge curves, the initial polarization at the beginning change is relatively large, leading to a low energy conversion efficiency of 85%. From the galvanostatic intermittent titration technique (GITT) result as shown in Figure S4 (Supporting Information), the OCV curve is overlapped with the second charge curve, indicating that this polarization is due to the slow $Na^+$ ion diffusion kinetics in the first charge process. However, after the first cycle, this polarization disappears and a higher energy conversion efficiency of 90% is demonstrated. The rate capability of the $Na_{0.9}[Cu_{0.22}Fe_{0.30}Mn_{0.48}]O_2$ electrode was also tested at different current rates from *C*/10 to 5 C. In Figure 2b, the reversible capacities are 98, 94, 88, 78, 72, and 59 mAh $g^{-1}$ at constant rates of 0.1C, 0.2C, 0.5C, 1C, 2C, and 5C, respectively. The capacity retention at 5C is 60% of the initial capacity in this micro-sized sample without optimization. The other appealing property is the long cycle life. As shown in Figure 2c, the cell is highly reversible; after 100 cycles, the capacity retention is 97% of its initial capacity, showing very stable cycling performance. Most importantly, the as-synthesized samples after soaked in water or stored in air were also tested in sodium half cells, whose electrochemical result is shown in Figures S3 and S5 (Supporting Information). It can be seen that there is almost no decay in the performance, although the Na content is slightly less than that of the as-synthesized sample (see Table S2, Supporting Information), indicating that the resulting material is stable against water and in air. For comparison, the as-synthesized O3-$NaFe_{1/2}Mn_{1/2}O_2$ sample is not stable against water (Figure S2, Supporting Information) and shows relatively large polarization in the charge and discharge curves (Figure S6, Supporting Information). All these results combined with electrochemical data demonstrate that the incorporation of Cu into the Fe/Mn transition metal layer not only enhances the stability but also improves the reversibility and kinetics (see Figure S6, Supporting Information). The reason might be that the incorporation of Cu into layered oxides either improves the average storage voltage which can avoid to be oxidized by water/oxygen/$CO_2$ or forms the different surface structures and compositions which protect the bulk material from direct contact with air (note that a thin layer of $Na_2CO_3$ is usually formed when most of the as-synthesized sodium layered oxides are exposed in air,

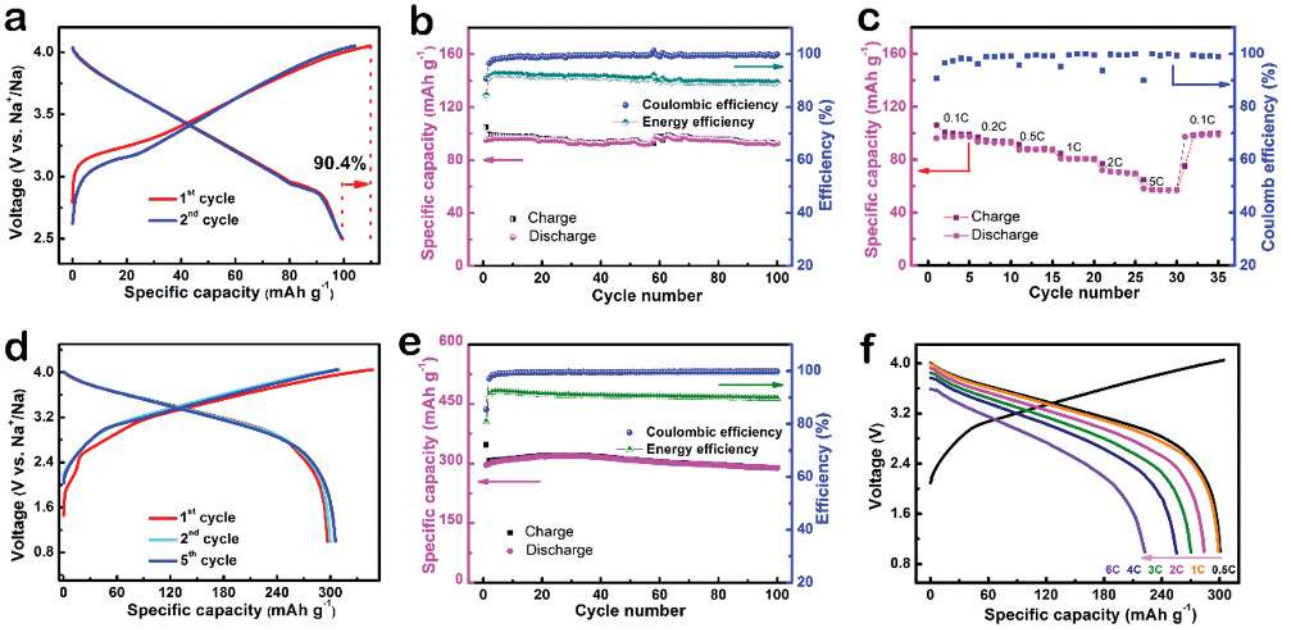


**Figure 2.** Na storage performance of the O3-$Na_{0.9}[Cu_{0.22}Fe_{0.30}Mn_{0.48}]O_2$ electrode (a–c). a) The first and second galvanostatic charge and discharge curves of the $Na_{0.9}[Cu_{0.22}Fe_{0.30}Mn_{0.48}]O_2$ electrode cycled between 2.5 and 4.05 V at a current rate of 0.1C (10 mA $g^{-1}$). b) Long-term cycling performance. The capacity, Coulombic efficiency, and energy conversion efficiency versus cycle number at a 0.1C rate. c) Rate capability. Capacity versus cycle number at various current rates from 0.1C to 5C. Na storage performance of the O3-$Na_{0.9}[Cu_{0.22}Fe_{0.30}Mn_{0.48}]O_2$//hard carbon full cells (d-f). d) The first, second, and fifth charge and discharge curves of the full cell cycled between 1 and 4.05 V at a 0.5C rate. e) Long-term cycling performance, the Coulombic efficiency, and the energy conversion efficiency versus cycle number at the 0.5C rate and f) rate capability. Discharge curves of the full cell cycled at constant charge/discharge rates from 0.5C to 6C (one charge curve at 0.5C rate is also shown). The specific capacities were calculated based on the mass of cathode material in (a–c) and based on the mass of anode material in (d–f).

which is similar to lithium layered oxides where a thin layer of $Li_2CO_3$ is always there. The problem is that $Na_2CO_3$ is soluble in water whereas $Li_2CO_3$ is not.)

The outstanding Na storage performance of the O3-$Na_{0.9}[Cu_{0.22}Fe_{0.30}Mn_{0.48}]O_2$ cathode material paves the way for constructing a prototype rechargeable sodium-ion battery using hard carbon as the anode[14] (see Figure S7, Supporting Information) and 0.8 M $NaPF_6$/EC:DMC (1:1 in volume; EC: ethylene carbonate; DMC: dimethyl carbonate) as the electrolyte in standard coin cells. The preliminary electrochemical results of the full cell in Figure 2d–f show that the reversible capacity is around 300 mAh $g^{-1}$ (based on the mass of the anode) at a current rate of 0.5C. A high average operation voltage of 3.2 V was achieved in this system. The Coulombic efficiency and round-trip energy efficiency of the first cycle are 85% and 80% and can be increased to 99% and 90% after initial cycles (note that the round-trip energy efficiency of this system is much higher than that of commercialized high-temperature Na—S battery which is now used in stationary energy storage (75%–85%)[2a]. The energy density of this system is calculated to be 210 Wh $kg^{-1}$ based on the total mass of cathode and anode. The other important feature of this system is the excellent cycling performance. As shown in Figure 2e, after 100 cycles, the full cell shows no capacity decay. In Figure 2f, the reversible capacities are 301, 299, 284, 270, 255, and 222 mAh $g^{-1}$ at the same charge–discharge rates of 0.5C, 1C, 2C, 3C, 4C, and 6C, respectively. When the full cell was charged at a 0.5C rate and discharged at various rates, much higher capacity retentions of 99% and 65% are achieved at 6C and 12C rates (10 and 5 min discharging) (see Figure S8, Supporting Information). These indicate that the battery is capable of discharging at a very high rate. The cost of this system could be much lower than other systems because inexpensive elements were used in the cathode material (note that the cost of copper oxide is only half of that of nickel oxide and one quarter of cobalt oxide). The other point is that the cheaper Al foil current collector was used for both cathode and anode in these full cells and an environmentally benign aqueous sodium alginate binder was used for the anode preparation, which leads to a further reduction in cost. These desired characteristics of this system that potentially meet the requirements for stationary energy storage are indeed closer to the level of practical applications.

To unravel the electrochemical Na deintercalation/intercalation mechanism in this O3-$Na_{0.9}[Cu_{0.22}Fe_{0.30}Mn_{0.48}]O_2$ material, we performed the electrochemical in situ XRD and ex situ X-ray absorption spectroscopy (XAS) experiments. **Figure 3** shows the XRD pattern evolution of the electrode cycled at 0.1 C rate in the voltage range of 2.5–4.1 V along with the in situ first charge and discharge curves. The peaks marked with asterisks at 38.4° and 44.7° belong to Al foil which was used as both current collector and X-ray window. Upon initial Na deintercalation, the (00*l*) peaks of the O3 phase first shift to lower angle and then a new peak which can be assigned to a hexagonal P3 phase appears at a lower angle,[5g] indicating a two-phase reaction with the coexistence of O3 and P3 phases in the voltage range of 3.2–3.3 V, corresponding to 0.10–0.15 Na deintercalation. Once the formation of P3 phase, the peaks for P3 phase show continuous shift until charged to 3.98 V without the appearance of

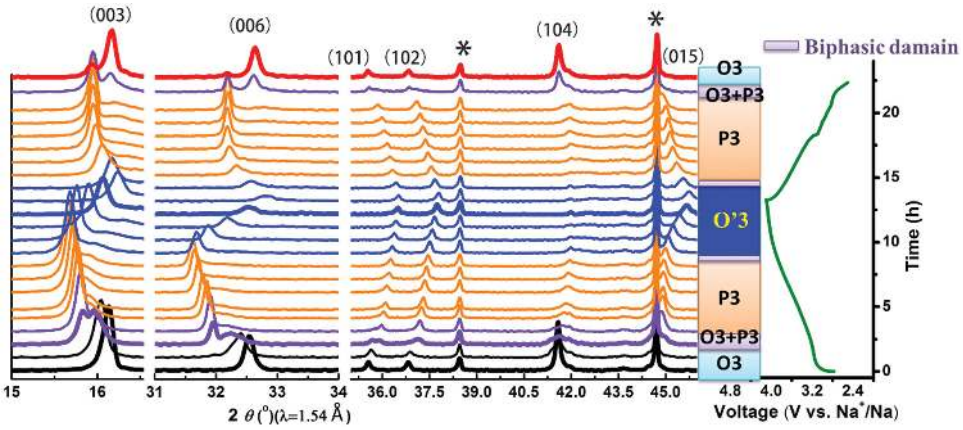


**Figure 3.** Structure evolution during electrochemical charge/discharge process. In situ XRD patterns collected during the first charge/discharge process of the O3-$Na_{0.9}[Cu_{0.22}Fe_{0.30}Mn_{0.48}]O_2$ electrode cycled between 2.5 and 4.1 V under a current rate of 0.1 C. Black asterisks represent peaks from Al window.

new peaks, indicating a solid–solution reaction in this region, which is consistent with the sloping changing curve. When further charged to the end, the P3 phase transforms to another new hexagonal O3 phase denoted as O'3 phase as the (00*l*) peaks shift back toward higher angle. The whole structure evolution is also illustrated in Figure 3. During discharge, the XRD pattern experiences an exact opposite evolution compared with charge process, indicating that the phase transition processes in the O3 material are highly reversible during the electrochemical Na deintercalation and intercalation in the initial cycle.

**Figure 4** displays the normalized X-ray absorption near-edge spectroscopy (XANES) spectra at the Cu, Fe, and Mn K-edges of the O3-$Na_{0.9}[Cu_{0.22}Fe_{0.30}Mn_{0.48}]O_2$ electrode with different charge and discharge states. The Cu K-edge spectrum shifts slightly to higher energy region upon charged to 4.1 V and shifts back after discharged to 2.5 V (Figure 4a,b), suggesting that $Cu^{2+}$ is oxidized to a higher valence. An even more pronounced change in the peak located at 8995 eV implies that the Cu–O local environment is significantly changed upon Na deintercalation and intercalation. Both reversible changes confirm

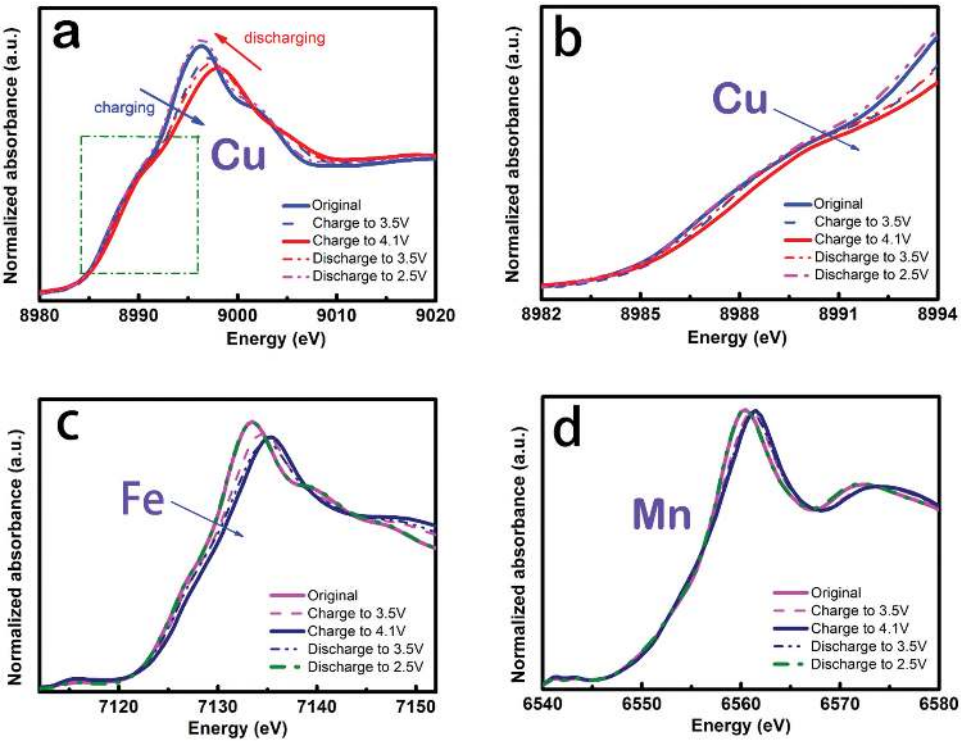


**Figure 4.** Charge compensation mechanism upon Na deintercalation/intercalation in O3-$Na_{0.9}[Cu_{0.22}Fe_{0.30}Mn_{0.48}]O_2$. a) Ex situ XANES spectra at Cu K-edge collected at different charge/discharge states, and b) the magnified region indicated by the rectangle in (a). c) Ex situ XANES spectra at Fe K-edge collected at different charge/discharge states, and d) ex situ XANES spectra at Mn K-edge collected at different charge/discharge states.

that copper is involved in the charge compensation during the electrochemical process. Furthermore, the Fe K-edge spectrum clearly shifts toward higher energy values with Na deintercalation, manifesting the oxidation of iron from $Fe^{3+}$ to $Fe^{4+}$, which is consistent with other iron-containing layered oxides.[7] In contrast, the change of Mn K-edge spectrum (Figure 4d) is not obvious during electrochemical cycling. Therefore, above results reveal that copper and iron are both electrochemically active and the redox couples of $Cu^{2+}/Cu^{3+}$ and $Fe^{3+}/Fe^{4+}$ are mainly responsible for the charge compensation mechanism,[10] which is consistent with the observed 0.4 $e^-$ transfer in the electrochemical process.

In conclusion, a highly efficient prototype sodium-ion battery was realized by using an air-stable and Co/Ni-free O3-$Na_{0.9}[Cu_{0.22}Fe_{0.30}Mn_{0.48}]O_2$ cathode and hard carbon anode. This 3.2 V class battery shows an energy density of 210 Wh $kg^{-1}$, a high round-trip energy efficiency of 90%, and excellent cycling stability. The battery is able to deliver 74% of initial capacity at a high charging/discharging current rate of 6C (i.e., 10 min). We believe that such outstanding performance of this prototype battery that is constructed from environmentally friendly and low-cost elements will pave the way for practical application in large-scale electrical energy storage.

## Supporting Information

Supporting Information is available from the Wiley Online Library or from the author.

## Acknowledgements

L.Q.M. and S.Y.X. contributed equally to this work. This work was supported by funding from the NSFC (51222210, 11234013, and 51421002) and the One Hundred Talent Project of the Chinese Academy of Sciences. The authors thank Yuesheng Wang for performing the XRD Rietveld refinement. The authors acknowledge the support by the staff scientists of Dr. Jingyuan Ma and Dr. Wen Wen at beam lines BL14W1 and BL14B1 of the Shanghai Synchrotron Radiation Facility (SSRF), China. The authors thank the BASF Company for providing the electrolyte solvents used in this work. Y.-S.H. conceived and designed this work; L.Q.M. performed all the synthesis and electrochemical experiments; S.Y.X. performed the accelerated aging experiment; L.Q.M. and S.Y.X. performed in situ XRD and ex situ XAS measurements; Y.M.L synthesized the negative electrode material; Y.-S.H. and L.Q.M. wrote the paper; all the authors participated in analysis of the experimental data and discussions of the results as well as preparing the paper.

Received: May 22, 2015
Revised: July 3, 2015
Published online: October 5, 2015

[1] a) K. Mizushima, P. C. Jones, P. J. Wiseman, J. B. Goodenough, *Mater. Res. Bull.* **1980**, *15*, 783; b) C. Delmas, J.-J. Braconnier, C. Fouassier, P. Hagenmuller, *Solid State Ionics* **1981**, *3*, 165.

[2] a) B. Dunn, H. Kamath, J.-M. Tarascon, *Science* **2011**, *334*, 928; b) Z. Yang, J. Zhang, M. C. Kintner-Meyer, X. Lu, D. Choi, J. P. Lemmon, J. Liu, *Chem. Rev.* **2011**, *111*, 3577; c) H. L. Pan, Y.-S. Hu, L. Q. Chen, *Energy Environ. Sci.* **2013**, *6*, 2338; d) V. Palomares, M. Casas-Cabanas, E. Castillo-Martínez, M. H. Han, T. Rojo, *Energy Environ. Sci.* **2013**, *6*, 2312; e) S.-W. Kim, D.-H. Seo, X. Ma, G. Ceder, K. Kang, *Adv. Energy Mater.* **2012**, *2*, 710; f) M. D. Slater, D. Kim, E. Lee, C. S. Johnson, *Adv. Funct. Mater.* **2013**, *23*, 947.

[3] a) J. Liu, K. Song, C. B. Zhu, C.-C. Chen, P. A. Aken, J. Maier, Y. Yu, *ACS Nano* **2014**, *8*, 7051; b) C. Zhu, K. Song, P. A. Aken, J. Maier, Y. Yu, *Nano Lett.* **2014**, *14*, 2175; c) Y.-L. Ding, Y. R. Wen, C. Wu, P. A. Aken, J. Maier, Y. Yu, *Nano Lett.* **2015**, *15*, 1388; d) Y. Wen, K. He, Y. J. Zhu, F. D. Han, Y. H. Xu, I. Matsuda, Y. Ishii, J. Cumings, C. S. Wang, *Nat. Commun.* **2014**, *5*, 4033.

[4] a) X. Ma, H. Chen, G. Ceder, *J. Electrochem. Soc.* **2011**, *158*, A1307; b) S. Komaba, C. Takei, T. Nakayama, A. Ogata, N. Yabuuchi, *Electrochem. Commun.* **2010**, *12*, 355; c) P. Vassilaras, X. Ma, X. Li, G. Ceder, *J. Electrochem. Soc.* **2013**, *160*, A207; d) S. Okada, Y. Takahashi, T. Kiyabu, T. Doi, J. Yamaki, T. Nishida, *ECS Meeting Abstr.* **2006**, MA2006–02201; e) M. Guignard, C. Didier, J. Darriet, P. Bordet, E. Elkaïm, C. Delmas, *Nat. Mater.* **2013**, *12*, 74; f) N. Yabuuchi, H. Yoshida, S. Komaba, *Electrochemistry* **2012**, *80*, 716; g) A. Mendiboure, C. Delmas, P. Hagenmuller, *J. Solid State Chem.* **1985**, *57*, 323; h) J. J. Braconnier, C. Delmas, P. Hagenmuller, *Mater. Res. Bull.* **1982**, *17*, 993.

[5] a) Z. Lu, J. R. Dahn, *J. Electrochem. Soc.* **2001**, *148*, A1225; b) D. Carlier, J. H. Cheng, R. Berthelot, M. Guignard, M. Yoncheva, R. Stoyanova, B. J. Hwang, C. Delmas, *Dalton Trans.* **2011**, *40*, 9306; c) H. Yoshida, N. Yabuuchi, S. Komaba, *Electrochem. Commun.* **2013**, *34*, 60; d) M. Sathiya, K. Hemalatha, K. Ramesha, J. M. Tarascon, A. S. Prakash, *Chem. Mater.* **2012**, *24*, 1846; e) D. Kim, E. Lee, M. Slater, W. Lu, S. Rood, C. S. Johnson, *Electrochem. Commun.* **2012**, *18*, 66; f) P. Vassilaras, A. J. Toumar, G. Ceder, *Electrochem. Commun.* **2014**, *38*, 79; g) X. Li, D. Wu, Y.-N. Zhou, L. Liu, X.-Q. Yang, G. Ceder, *Electrochem. Commun.* **2014**, *49*, 51; h) H. Yu, S. Guo, Y. Zhu, M. Ishida, H. S. Zhou, *Chem. Commun.* **2014**, *50*, 457.

[6] a) D. Kim, Sun-Ho Kang, M. Slater, S. Rood, J. T. Vaughey, N. Karan, M. Balasubramanian, C. S. Johnson, *Adv. Energy Mater.* **2011**, *1*, 333; b) N. Yabuuchi, M. Yano, H. Yoshida, S. Kuze, S. Komaba, *J. Electrochem. Soc.* **2013**, *160*, A3131; c) S. Komaba, N. Yabuuchi, T. Nakayama, A. Ogata, T. Ishikawa, I. Nakai, *Inorg. Chem.* **2012**, *51*, 6211; d) D. Yuan, X. Hu, J. F. Qian, F. Pei, F. Wu, R. Mao, X. Ai, H. Yang, Y. Cao, *Electrochem. Acta* **2014**, *116*, 300; e) S. Guo, H. Yu, L. Pan, Y. Ren, T. Zhang, M. Chen, M. Ishida, H. Zhou, *Energy Environ. Sci.* **2015**, *8*, 1237; f) X. Sun, Y. Jin, C.-Y. Zhang, J.-W. Wen, Y. Shao, Y. Zang, C.-H. Chen, *J. Mater. Chem. A* **2014**, *2*, 17268; g) D. Yuan, W. He, F. Wu, Y. Wu, J. Qian, Y. Cao, X. Ai, H. Yang, *J. Mater. Chem. A* **2013**, *1*, 3895; h) X. Wang, M. Tamaru, M. Okubo, A. Yamada, *J. Phys. Chem. C* **2013**, *117*, 15545.

[7] a) J. Thorne, R. Dunlap, M. Obrovac, *J. Electrochem. Soc.* **2013**, *160*, A361; b) B. M. de Boisse, D. Carlier, M. Guignard, C. Delmas, *J. Electrochem. Soc.* **2013**, *160*, A569; c) M. Yoncheva, R. Stoyanova, E. Zhecheva, E. Kuzmanova, M. Sendova-Vassileva, D. Nihtianova, D. Carlier, M. Guignard, C. Delmas, *J. Mater. Chem.* **2012**, *22*, 23418; d) N. Yabuuchi, M. Kajiyama, J. Iwatate, H. Nishikawa, S. Hitomi, R. Okuyama, R. Usui, Y. Yamada, S. Komaba, *Nat. Mater.* **2012**, *11*, 512; e) B. M. de Boisse, J. H. Cheng, D. Carlier, M. Guignard, C. J. Pan, S. Bordere, D. Filimonov, C. Drathen, E. Suard, B. J. Hwang, A. Wattiaux, C. Delmas, *J. Mater. Chem. A* **2015**, *3*, 10976; f) J. Zhao, J. Xu, D. H. Lee, N. Dimov, Y. S. Meng, S. Okada, *J. Power Sources* **2014**, *264*, 235.

[8] a) E. Lee, J. Lu, Y. Ren, X. Luo, X. Zhang, J. Wen, D. Miller, A. DeWahl, S. Hackney, B. Key, *Adv. Energy Mater.* **2014**, *4*, 1400458; b) K. Kubota, N. Yabuuchi, H. Yoshida, M. Dahbi, S. Komaba, *MRS Bull.* **2014**, *39*, 416; c) Y. Lei, X. Li, L. Liu, G. Ceder, *Chem. Mater.* **2014**, *26*, 5288; d) R. Kataoka, T. Mukai, K. Nakatani, A. Yoshizawa, T. Sakai, *J. Electrochem. Soc. Abstr.* **2012**, MA2012-021841.

[9] a) D. Buchholz, C. Vaalma, L. G. Chagas, S. Passerini, *J. Power Sources* **2015**, *282*, 581; b) N. Yabuuchi, R. Hara, K. Kubota,

J. Paulsen, S. Kumakura, S. J. Komaba, *J. Mater. Chem. A* **2014**, *2*, 16851; c) J. Xu, D. H. Lee, R. J. Clément, X. Yu, M. Leskes, A. J. Pell, G. Pintacuda, X.-Q. Yang, C. P. Grey, Y.-S. Meng, *Chem. Mater.* **2014**, *26*, 1260; d) N. Yabuuchi, R. Hara, M. Kajiyama, K. Kubota, T. Ishigaki, A. Hoshikawa, S. Komaba, *Adv. Energy Mater.* **2014**, *4*, 1614; e) S.-M. Oh, S.-T. Myung, J.-Y. Hwang, B. Scrosati, K. Amine, Y.-K. Sun, *Chem. Mater.* **2014**, *26*, 6165; f) D. W. Han, J. H. Ku, R. H. Kim, D. J. Yun, S. S. Lee, S. G. Doo, *ChemSusChem* **2014**, *7*, 1870; g) B. Juliette, S. Gurpreet, A. Robert, G. Elena, R. Vladimir, M. Armand, R. Teófilo, G. B. Peter, *Energy Environ. Sci.* **2014**, *7*, 1387; h) R. Kataoka, T. Mukai, A. Yoshizawa, T. Sakai, *J. Electrochem. Soc.* **2013**, *160*, A933.

[10] a) S. Y. Xu, X. Y. Wu, Y. M. Li, Y.-S. Hu, L. Q. Chen, *Chin. Phys. B* **2014**, *23*, 118202; b) L. Q. Mu, Y.-S. Hu, L. Q. Chen, *Chin. Phys. B* **2015**, *3*, 038203; c) Y. M. Li, Z. Z. Yang, S. Y. Xu, L. Q. Mu, L. Gu, Y.-S. Hu, H. Li, L. Q. Chen, *Adv. Sci.* **2015**, *2*, 1500031.

[11] D. Buchholz, C. Gomes, V. Christoph, W. Liming, P. Stefano, *J. Mater. Chem. A* **2014**, *33*, 13415.

[12] V. Duffort, E. Talaie, R. Black, L. F. Nazar, *Chem. Mater.* **2015**, *33*, 13415.

[13] C. Delmas, C. Fouassier, P. Hagenmuller, *Phys. B+C* **1980**, *99*, 81.

[14] Y. M. Li, S. Y. Xu, X. Y. Wu, J. Z. Yu, Y. S. Wang, Y.-S. Hu, H. Li, L. Q. Chen, X. J. Huang, *J. Mater. Chem. A* **2015**, *3*, 71.